Study on dispersion-induced phase noise in an optical OFDM radio-over-fiber system at 60-GHz band

Chia Chien Wei[1,*] and Jason (Jyehong) Chen[2]

[1]*Department of Applied Materials and Optoelectronic Engineering, National Chi Nan University, 1 University Rd., Puli, Nautou, 545, Taiwan*

[2]*Department of Photonics and Institute of Electro-Optical Engineering, National Chiao-Tung University, 1001 Ta Hsueh Rd., Hsin-Chu, 300, Taiwan*

**ccwei@ncnu.edu.tw*

Abstract: While coherency between an RF-tone and OFDM signals in RoF systems at 60 GHz is de-correlated by fiber dispersion, both phase rotation term (PRT) on each subcarrier and inter-carrier interference (ICI) between subcarriers are induced at a receiver. We analytically calculate the powers of PRT and ICI under different parameters, such as subcarrier number, modulation format, laser linewidth and transmission distance. Moreover, dispersion-induced ICI is shown to be non-Gaussian distributed by its kurtosis, and its distribution depends on system parameters. Therefore, using only the power of ICI cannot predict accurate bit error rate (BER) and corresponding power penalty. We propose to use *t*-distribution to fit the distribution of ICI, and it can be used to compute BER precisely.

OCIS codes: (060.2330) Fiber optics communications; (060.5625) Radio frequency photonics

References and links

1. M. Sauer, A. Kobyakov, and J. George, "Radio over fiber for picocellular network architectures," J. Lightwave Technol. **25**(11), 3301–3320 (2007).
2. A. M. J. Koonen, and L. M. Garcia, "Radio-over-MMF techniques – part II: microwave to millimeter-wave systems," J. Lightwave Technol. **26**(15), 2396–2408 (2008).
3. Y. X. Guo, B. Luo, C. S. Park, L. C. Ong, M.-T. Zhou, and S. Kato, "60 GHz radio-over-fiber for Gbps transmission," in Proc. Global Symp. Millimeter Waves (GSMM), 41–43 (2008).
4. H.-C. Chien, A. Chowdhury, Z. Jia, Y.-T. Hsueh, and G.-K. Chang, "60 GHz millimeter-wave gigabit wireless services over long-reach passive optical network using remote signal regeneration and upconversion," Opt. Express **17**, 3016–3024 (2009), http://www.opticsinfobase.org/oe/abstract.cfm?uri=oe- 17-5-3016.
5. C. T. Lin, E. Z. Wong, W. J. Jiang, P. T. Shih, J. Chen, and S. Chi, "28-Gb/s 16-QAM OFDM radio-over-fiber system within 7-GHz license-free band at 60 GHz employing all-optical up-conversion," in *Proc. CLEO 2009*, Maryland, Baltimore, CPDA8 (2009).
6. Z. Jia, J. Yu, Y.-T. Hsueh, A. Chowdhury, H.-C. Chien, J. A. Buck, and G.-K. Chang, "Multiband signal generation and dispersion-tolerant transmission based on photonic frequency tripling technology for 60-GHz radio-over-fiber systems," IEEE Photon. Technol. Lett. **20**(17), 1470–1472 (2008).
7. C.-T. Lin, J. Chen, P.-T. Shih, W.-J. Jiang, and S. Chi, "Ultra-high data-rate 60 GHz radio-over-fiber systems employing optical frequency multiplication and OFDM formats," J. Lightwave Technol. **28**(16), 2296–2306 (2010).
8. J. Armstrong, "OFDM for optical communications," J. Lightwave Technol. **27**(3), 189–204 (2009).
9. Z. Zan, M. Premaratne, and A. J. Lowery, "Laser RIN and linewidth requirements for direct detection optical OFDM," in *Proc. CLEO'08*, San Jose, CWN2 (2008).
10. W.-R. Peng, J. Chen, and S. Chi, "On the phase noise impact in direct-detection optical OFDM transmission," IEEE Photon. Technol. Lett. **22**(9), 649–651 (2010).
11. C.-T. Lin, P.-T. Shih, J. Chen, W.-Q. Xue, P.-C. Peng, and S. Chi, "Optical millimeter-wave signal generation using frequency quadrupling technique and no optical filtering," IEEE Photon. Technol. Lett. **20**(12), 1027–1029 (2008).
12. P.-T. Shih, J. Chen, C.-T. Lin, W.-J. Jiang, H.-S. Huang, P.-C. Peng, and S. Chi, "Optical millimeter-wave signal generation via frequency 12-tupling," J. Lightwave Technol. **28**(1), 71–78 (2010).
13. K. Higuma, S. Oikawa, Y. Hashimoto, H. Nagata, and M. Izutsu, "X-cut lithium niobate optical single-sideband

#133218 - $15.00 USD Received 11 Aug 2010; revised 7 Sep 2010; accepted 7 Sep 2010; published 15 Sep 2010

modulator," Electron. Lett. **37**(8), 515–516 (2001).
14. M. S. El-Tanany, Y. Wu, and L. Hazy, "Analytical modeling and simulation of phase noise interference in OFDM-based digital television terrestrial broadcasting systems," IEEE Trans. Broadcast **47**(1), 20–31 (2001).
15. X. Yi, W. Shieh, and Y. Ma, "Phase noise effects on high spectral efficiency coherent optical OFDM systems," J. Lightwave Technol. **26**(10), 1309–1316 (2008).
16. D. Petrovic, W. Rave, and G. Fettweis, "Properties of the intercarrier interference due to phase noise in OFDM," in *Proc. ICC'05*, 2605–2610 (2005)
17. E. Costa, and S. Pupolin, "M-QAM-OFDM system performance in the presence of a nonlinear amplifier and phase noise," IEEE Trans. Commun. **50**(3), 462–472 (2002).
18. K. Pearson, "Contributions to the mathematical theory of evolution. II. skew variation in homogeneous material," Philos. Trans. Roy. Soc. London Ser. A **186**(0), 343–414 (1895).

1. Introduction

Due to the limited wireless spectrum, current data rate of tens of Mbps in wireless communications is not enough for the rising demand for higher data rate. To develop popular bandwidth-hungry applications, such as High-Definition (HD) video, mm-wave is a good candidate to carry signals of multi-Gbps. For instance, the FCC's 60-Hz band offers 7 GHz of unlicensed spectrum (57- 64 GHz) [1]. However, because of the significantly high air-link loss at 60 GHz (8~8.5 dB/m in modern office building) and higher noise power due to wide channel bandwidth, the radio cells at 60 GHz are typically smaller than 10 m [2, 3]. Consequently, extensive high-capacity feeders, such as optical fibers in Radio-over-Fiber (RoF) systems, are needed to interconnect radio access points [4–7].

Orthogonal-frequency-division-multiplexing (OFDM) is a promising modulation format for broadband wireless communication systems owing to its robustness against the inter-symbol interference caused by both multipath in air-link and chromatic dispersion (CD) in optical fibers [8]. To generate electrical OFDM signals at 60-GHz band at a receiver, an RF-tone and optical OFDM signals with 60-GHz frequency difference have to be sent into fiber simultaneously, and the beating term between the RF-tone and optical OFDM signals after a photo-detector is the desired electrical OFDM signals [4–7]. Theoretically, both the RF-tone and optical OFDM signals are generated by modulating the same laser to eliminate the performance degradation caused by laser phase noise (PN). However, because the optical OFDM signals and the RF-tone will walk off due to their different group velocities in fiber, their phase coherency is losing, and PN is generated in detection as a result. Compared with direct-detection optical OFDM signals [9, 10], the larger frequency difference of 60 GHz will cause more PN in a shorter transmission distance, especially when a cost-effective commercial DFB laser with linewidth of several MHz is adopted in OFDM RoF systems. Moreover, the dispersion-induced PN not only creates a phase rotation term (PRT) on each subcarrier, but also causes inter-carrier interference (ICI) between subcarriers [10]. Notably, the PRTs of subcarriers are not exactly identical, because the optical OFDM subcarriers occupy different frequency bands resulting in different group delays.

In this work, we analytically calculate the powers of PRT and ICI, and compute kurtosis to show the ICI induced by dispersion is non-Gaussian distributed. Non-Gaussian distribution implies that the signal-to-noise ratio (SNR) cannot predict bit error rate (BER) well. Accordingly, a distribution with variable kurtosis is required to simulate a non-Gaussian distribution. While *t*-distribution is a suitable candidate, it can be used to compute BER precisely under different parameters, such as subcarrier number, modulation format and transmission distance.

#133218 - $15.00 USD Received 11 Aug 2010; revised 7 Sep 2010; accepted 7 Sep 2010; published 15 Sep 2010

2. System model

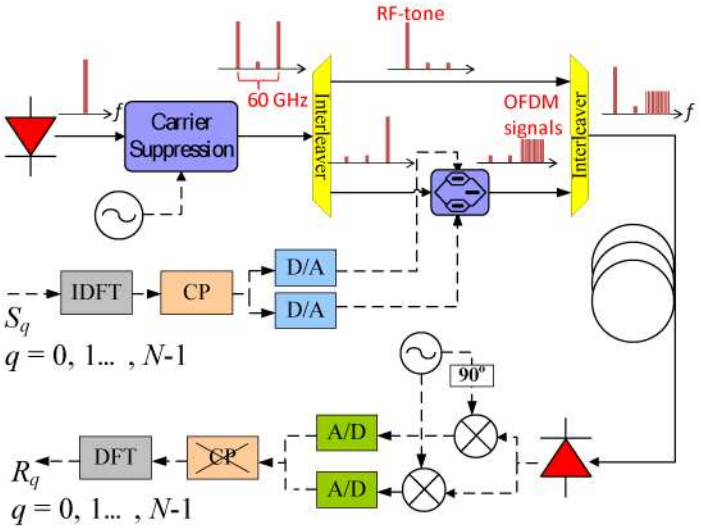

Fig. 1. OFDM RoF transmission at 60-GHz band

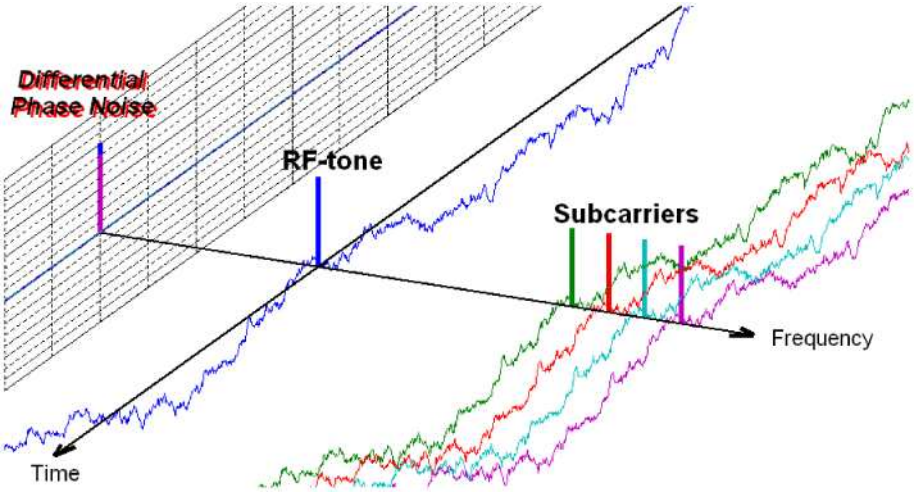

Fig. 2. Schematic plot of dispersion-induced phase difference between the RF-tone and subcarriers. (Media 1)

Figure 1 depicts the setup of an OFDM RoF system at 60-GHz band. At the transmitter, a laser source is modulated into two coherent monochromatic tones with 60-GHz frequency difference [11, 12]. When one of them is used as the RF-tone without further modulation, the other will be modulated by an optical I/Q modulator to carry complex OFDM signals [13]. Although various architectures can realize identical optical single-sideband OFDM RoF signals [5–7], the advantages and disadvantages of different architectures will not be included in this work. While coherent RF-tone and OFDM signals with frequency difference of 60 GHz are generated, electrical OFDM signals at 60-GHz band can be obtained at the receiver by square-law detection. After down conversion, removing the cyclic prefix (CP) and taking discrete Fourier transform (DFT), the received qth subcarrier in an OFDM symbol without transmission is given as,

$$R_q = H_q S_q + W_q , \tag{1}$$

#133218 - $15.00 USD Received 11 Aug 2010; revised 7 Sep 2010; accepted 7 Sep 2010; published 15 Sep 2010

where S_q, H_q and W_q are the transmitted data, the channel response and the white noise at the qth subcarrier. Since the proper cyclic prefix is added at the transmitter, CD of fiber only affects the phase of the channel response. However, the PN induced by different group delays is not considered in Eq. (1). Since the subcarrier number of OFDM signals, N, is usually large to make each subcarrier bandwidth small, in order to be tolerant to uneven frequency response, each subcarrier can be treated as a monochromatic carrier for simplicity, as shown in Fig. 2. Consequently, while the RF-tone and the OFDM subcarriers propagate in fiber with different group velocities, the phase difference between the RF-tone and the qth subcarrier can be simply approximated as $\varphi_q(t) = \theta(t+t_q) - \theta(t)$. $\theta(t)$ is the laser phase modeled by the Wiener process [14], and t_q is the relative time delay between the RF-tone and the qth subcarrier. Hence, φ_q is Gaussian distributed with the variance of $2\pi\beta t_q$, while β is the 3-dB laser linewidth. Considering the discrete frequency component of $\exp\left(j\varphi_q(t)\right)$:

$$I_q(k) = \frac{1}{N}\sum_{n=0}^{N-1} e^{j\varphi_q(n)} e^{-j\frac{2\pi}{N}nk}, \tag{2}$$

where $\varphi_q(n) \equiv \varphi_q(n\Delta t)$ is the sampled phase difference at the sampling rate of $1/\Delta t$, the PN will not only affect the qth subcarrier by $I_q(0)$, but also expand in frequency domain to interfere neighboring subcarriers by $I_q(k)\big|_{k\neq 0}$. Accordingly, Eq. (1) should be modified as [10],

$$R_q = H_q S_q I_q(0) + \sum_{\substack{m=0 \\ m\neq q}}^{N-1} H_m S_m I_m(q-m) + W_q . \tag{3}$$

Since PN is typically small, $I_q(0)$ can be approximated as $\exp(j\bar{\varphi}_q)$ [15], where,

$$\bar{\varphi}_q = \frac{1}{N}\sum\nolimits_{n=0}^{N-1} \varphi_q(n) . \tag{4}$$

As a result, $I_q(0)$ provides a PRT, $\bar{\varphi}_q$, on the qth subcarrier, and $\bar{\varphi}_q$ varies from a subcarrier to another one. In addition to the PRT, ICI described by the second term of Eq. (3) is contributed by the other subcarriers, and it will also distort the received data.

3. The properties of PRT and ICI

Using the autocorrelation of φ_q: $\left\langle \varphi_q(n)\varphi_q(n+\Delta n)\right\rangle = 2\pi\beta\max\left(0, t_q - |\Delta n|\Delta t\right)$ [14], the variance of $\bar{\varphi}_q$ can be derived as,

$$\sigma^2_{\mathrm{PRT}}(q) = \frac{2\pi\beta}{N^2}\left[Nt_q + 2\sum_{\Delta n=1}^{n_q}\left(N-\Delta n\right)\left(t_q - \Delta n\,\Delta t\right)\right], \tag{5}$$

where $n_q = \min\left(N-1, \lfloor t_q/\Delta t \rfloor\right)$, and $\lfloor x \rfloor$ indicates the largest integer $\leq x$. Moreover, assuming that $\left\langle |H_q|^2\right\rangle = 1$ and $\left\langle S_q S^*_{q'}\right\rangle = P_S\,\delta(q-q')$, and the normalized power of ICI can be represented as:

#133218 - $15.00 USD Received 11 Aug 2010; revised 7 Sep 2010; accepted 7 Sep 2010; published 15 Sep 2010

$$\tilde{\sigma}^2_{\mathrm{ICI}}(q) = \frac{\sigma^2_{\mathrm{ICI}}(q)}{P_S} = \sum_{\substack{m=0 \\ m\neq q}}^{N-1} \left\langle |I_m(q-m)|^2 \right\rangle . \tag{6}$$

To proceed, $|I_m(k)|^2$ is rewritten as

$$\left|I_m(k)\right|^2 = \frac{1}{N^2} \sum_{\Delta n=1-N}^{N-1} f_m(\Delta n) \cdot e^{-j\frac{2\pi}{N}\Delta n k},$$

where

$$f_m(\Delta n) = \sum_{k=|\Delta n|}^{N-1} e^{\mathrm{sgn}(\Delta n)\cdot j\left(\varphi_m(k)-\varphi_m(k-|\Delta n|)\right)} .$$

Because of $\langle \exp(jA) \rangle = \exp\left(-\langle A^2 \rangle / 2\right)$, where A is a random variable, the $\langle f_m(\Delta n) \rangle$ is derived as $\left(N-|\Delta n|\right)\times \exp\left(-2\pi\beta \cdot \min\left(|\Delta n|\Delta t, t_m\right)\right)$ and we have,

$$\left\langle \left|I_m(k)\right|^2 \right\rangle = \frac{1}{N} + \frac{2}{N^2} \sum_{\Delta n=1}^{N-1} \left(N-\Delta n\right) \cos\left(\frac{2\pi}{N}\Delta n\, k\right) e^{-2\pi\beta \min\left(\Delta n \Delta t,\, t_m\right)} . \tag{7}$$

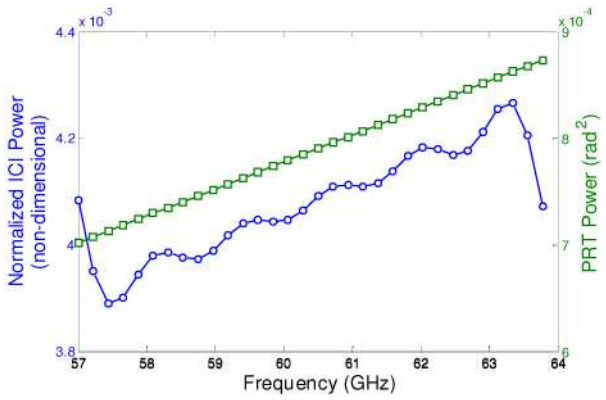

Fig. 3. The ICI and PRT powers of OFDM signals over 32 subcarriers with 1-MHz laser linewidth after 100-km transmission.

Since this work focus on the case of OFDM signals at unlicensed band within 57 GHz and 64 GHz, the dispersion-induced relative time delay is set as $t_q = DLc/\lambda^2 \times \left(f_0 + \Delta f \times q/N\right)$, where $D = 16$ ps/nm/km is the dispersion parameter, $\lambda = 1550$ nm is the signal wavelength, c is the light speed, L is the transmission distance, and the frequency difference between the first (last) subcarrier and the RF-tone is $f_0 = 57$ GHz ($f_0 + \Delta f = 64$ GHz). Figure 3 shows ICI power and PRT power of OFDM signals over 32 subcarriers calculated by Eqs. (5)-(7), and each subcarrier has different noise power due to different group delay. In Fig. 3, higher frequency corresponding to more relative group delay results in more differential PN and higher PRT power. Nevertheless, since $\left\langle |I_m(k)|^2 \right\rangle$ is a circular function and $\tilde{\sigma}^2_{\mathrm{ICI}}(N-1)$ is mainly contributed by $\left\langle |I_{N-2}(1)|^2 \right\rangle$ (high relative group delay) and $\left\langle |I_0(-1)|^2 \right\rangle$ (low relative group delay), $\tilde{\sigma}^2_{\mathrm{ICI}}(N-1)$ is lower than $\tilde{\sigma}^2_{\mathrm{ICI}}(N-2)$. However, higher frequency basically corresponds to higher ICI power.

#133218 - $15.00 USD Received 11 Aug 2010; revised 7 Sep 2010; accepted 7 Sep 2010; published 15 Sep 2010

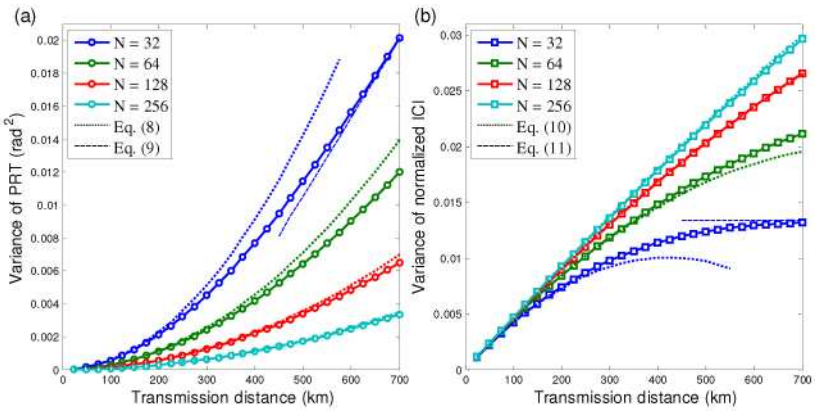

Fig. 4. Variances of (a) PRT and (b) normalized ICI for with 1-MHz linewidth

According to Eqs. (5)-(7), Fig. 4 plots the theoretical values of $\sigma^2_{\mathrm{PRT}}(N/2)$ and $\tilde{\sigma}^2_{\mathrm{ICI}}(N/2)$ with β of 1 MHz. The OFDM signals over fewer subcarriers show lower ICI power but higher PRT power, and the PRT power increases faster than ICI power as CD increasing. Therefore, both of them have to be considered to evaluate the transmission performance. Furthermore, while the relative group delay is small and $t_q << N\Delta t$, $\sigma^2_{\mathrm{PRT}}(q)$ can be approximated as,

$$\sigma^2_{\mathrm{PRT}}(q) \underset{n_q<<N}{\cong} 2\pi\beta\left[t_q\left(2n_q+1\right)-n_q\Delta t\left(n_q+1\right)\right]\underset{t_q\cong n_q\Delta t}{\cong}\frac{2\pi\beta t_q^2}{N\Delta t}. \tag{8}$$

Under this condition, PRT is proportional to the square of the relative time delay which is determined by the transmission distance and its frequency difference from the RF-tone. Additionally, PRT is inverse proportional to the subcarrier number. Furthermore, if the relative group delay is large and $t_q > N\Delta t$, Eq. (5) becomes

$$\sigma^2_{\mathrm{PRT}}(q) \underset{n_q=N}{=} 2\pi\beta\left[t_q-\frac{N(N^2-1)}{3N^2}\Delta t\right]\underset{N^2>>1}{\cong}2\pi\beta\left(t_q-\frac{N\Delta t}{3}\right), \tag{9}$$

and PRT is proportional to the relative time delay.

For simplicity, although ICI is contributed by the other subcarriers at different frequencies, we may assume their relative time delays are similar due to the small signal bandwidth (7 GHz) compared with the radio frequency (60 GHz). As a result, Eq. (4) can be approximated as,

$$\tilde{\sigma}^2_{\mathrm{ICI}}(q) \underset{t_m=t_q}{\cong}\sum_{\substack{m=0\\ m\neq q}}^{N-1}\left\langle|I_q(q-m)|^2\right\rangle = 1-\left\langle|I_q(0)|^2\right\rangle.$$

The second equality of the above equation is derived from $\sum_{m=0}^{N-1}\left\langle|I_q(m)|^2\right\rangle=1$ [16]. According to Eq. (7) and using the first-order approximation,

$$\tilde{\sigma}^2_{\mathrm{ICI}}(q)\cong 1-\frac{1}{N}-\frac{2}{N^2}\left[\sum_{\Delta n=1}^{n_q}\left(1-2\pi\beta\Delta n\Delta t\right)\left(N-\Delta n\right)+\left(1-2\pi\beta t_q\right)\sum_{\Delta n=n_q+1}^{N-1}\left(N-\Delta n\right)\right]$$

$$=\frac{2\pi\beta}{N^2}\left[\left(N-n_q-1\right)\left(N-n_q\right)t_q+\left(N-\frac{2n_q+1}{3}\right)\left(n_q+1\right)n_q\Delta t\right].$$

#133218 - $15.00 USD Received 11 Aug 2010; revised 7 Sep 2010; accepted 7 Sep 2010; published 15 Sep 2010

As a result, when the relative group delay is small and $n_q << N$, the normalized ICI power is,

$$\tilde{\sigma}^2_{\mathrm{ICI}}(q) \underset{t_q \equiv n_q \Delta t}{\cong} 2\pi\beta t_q \left(1 - \frac{t_q}{N\Delta t}\right) \tag{10}$$

which is proportional to the relative time delay and depends on the subcarrier number little. However, if the relative group delay is large and $n_q = N-1$, the ICI becomes

$$\tilde{\sigma}^2_{\mathrm{ICI}}(q) \underset{N^2 >> 1}{\cong} \frac{2\pi\beta N\Delta t}{3}. \tag{11}$$

In this case, ICI is proportional to the subcarrier number, but it is independent on the relative time delay implying that it does not increase as further extending the transmission distance. This approximated results of Eqs. (9) and (11) are identical to the results in coherent-detected OFDM systems [17], since large group delay makes the RF-tone and OFDM signals to be completely incoherent. Moreover, Eqs. (8) and (10) are plotted by the dotted lines in Figs. 4(a) and (b) for comparison, respectively. However, the dashed lines representing Eqs. (9) and (11) only show the case of $N = 32$ in Figs. 4(a) and (b), because $t_q / \Delta t$ is only about 38 after transmission of 700 km.

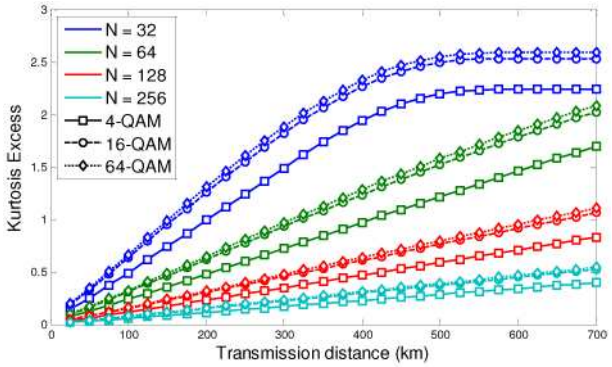

Fig. 5. The kurtosis excess of the real part of ICI

From Eq. (4), PRT is approximated as the summation of Gaussian distributed random variables, and therefore, it is also Gaussian distributed. However, according to Eq. (3), since ICI is the summation of independent but non-identical distributed random variables, the central limit theory cannot be applied, and ICI may not be normally distributed. Actually, ICI is not Gaussian distributed, and this can be shown by calculating its kurtosis excess. The definition of kurtosis excess, γ_2, is $\mu_4 / \sigma^4 - 3$, where μ_4 is the forth central moment and σ^2 is the variance. For a normal distribution, μ_4 is $3\sigma^2$, and therefore, γ_2 is zero. While the real and imaginary parts of ICI have independent and identical distribution, the kurtosis excess of the real part (or imaginary part) can be derived as $2\left\langle |\mathrm{ICI}|^4 \right\rangle / \left\langle |\mathrm{ICI}|^2 \right\rangle^2 - 4$:

$$\gamma_{2,\mathrm{ICI}}(q) = \frac{2\left\langle |S_m|^4 \right\rangle}{\tilde{\sigma}^4_{\mathrm{ICI}}(q) P_S^2} \sum_{\substack{m=0 \\ m\neq q}}^{N-1} \left\langle |I_m(q-m)|^4 \right\rangle + \frac{4}{\tilde{\sigma}^4_{\mathrm{ICI}}(q)} \sum_{\substack{m=0 \\ m\neq q}}^{N-1} \sum_{\substack{m'=0 \\ m'\neq q,m}}^{N-1} \left\langle |I_m(q-m) I_{m'}(q-m')|^2 \right\rangle - 4 . \tag{12}$$

The results of Eq. (12) with $q = N/2$ are plotted in Fig. 5. For ICI, fewer subcarriers and higher dispersion will result in higher kurtosis and more deviation from a normal distribution.

#133218 - $15.00 USD Received 11 Aug 2010; revised 7 Sep 2010; accepted 7 Sep 2010; published 15 Sep 2010

Moreover, since $\left\langle |X_m|^4 \right\rangle / P_S^2$ depends on its modulation format, such as 1 for 4-QAM and 1.32 for 16-QAM, $\gamma_{2,\mathrm{ICI}}$ are slightly different for different formats.

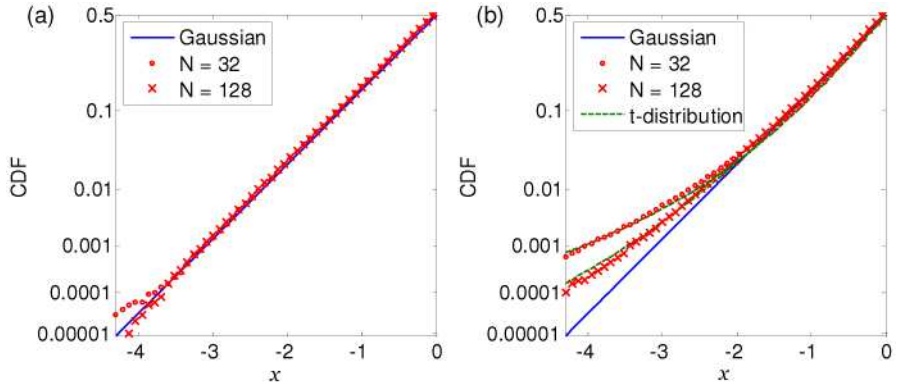

Fig. 6. Normalized CDF of (a) PRT and (b) the real part of ICI for 16-QAM OFDM signals

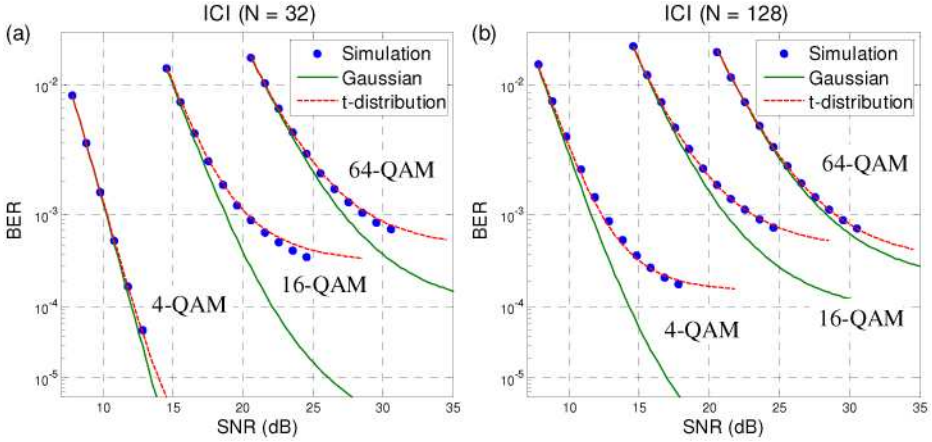

Fig. 7. BER curves of OFDM signals over (a) 32 subcarriers and (b) 128 subcarriers after 1400 km (4-QAM), 350 km (16-QAM) and 87.5 km (64-QAM) SMF transmission with 1-MHz laser linewidth.

To compare the distributions more directly, Fig. 6 shows numerical simulation results of the normalized cumulative distribution functions (CDF). The normalized CDFs of PRT and the real part of ICI are plotted in Fig. 6(a) and (b), respectively, and the transmission distance and the laser linewidth are 350 km and 1 MHz. The scales of vertical axes in Fig. 6 are adjusted to make the CDF of a normal distribution linear. For ICI, $\gamma_{2,\mathrm{ICI}}(N/2)$ are about 2 and 0.5 with $N = 32$ and 128, and their cumulative densities are about 100 and 10 times higher than that of a normal distribution at $x = -4.3$. Furthermore, Fig. 6(a) demonstrates that the distribution of PRT fits a normal distribution well. Hence, to estimate the influence of ICI by Gaussian approximation may underestimate corresponding signal degradation. Figure 7 shows the BER curves of theoretical prediction for rectangular *M*-ary QAM ($\log_2 M$ is even), the ICI of which is assumed to be a normal distribution, and the BER is calculated by [10],

$$\mathrm{BER} = \frac{8}{NM\log_2 M}\sum_{q=0}^{N-1}\int_{-\pi}^{\pi}\frac{e^{-\frac{\theta^2}{2\sigma_{\mathrm{PRT}}^2(q)}}}{\sqrt{2\pi}\sigma_{\mathrm{PRT}}(q)}\left[\sum_{k,k'=1}^{\sqrt{M}/2}\mathrm{Q}\left(\eta\cdot\Theta_{k,k'}(\theta)\right)+\sum_{\substack{k,k'=1\\ k\neq\sqrt{M}/2}}^{\sqrt{M}/2}\mathrm{Q}\left(\eta\cdot\hat{\Theta}_{k,k'}(\theta)\right)\right]\mathrm{d}\theta, \quad (13)$$

#133218 - $15.00 USD Received 11 Aug 2010; revised 7 Sep 2010; accepted 7 Sep 2010; published 15 Sep 2010

where

$$\eta = \sqrt{\frac{3}{M-1}\left(\rho^{-1} + \tilde{\sigma}_{\mathrm{ICI}}^2(q)\right)^{-1}}\,, \tag{14}$$

$$\Theta_{k,k'}(\theta) = (2k-1)\cos\theta - (2k'-1)\sin\theta - 2(k-1)\,, \tag{15}$$

$$\hat{\Theta}_{k,k'}(\theta) = -(2k-1)\cos\theta + (2k'-1)\sin\theta + 2k\,, \tag{16}$$

$\mathrm{Q}(x) = \mathrm{erfc}\left(x/\sqrt{2}\right)/2$ is a normalized form of the cumulative normal distribution function, and $\rho = P_S \Big/ \left\langle |W_q|^2 \right\rangle$ is the SNR. Numerical simulation results are plotted in Fig. 7 to show the estimation error by setting ICI Gaussian-distributed. The estimation error will increase as $\gamma_{2,\mathrm{ICI}}$ or $\tilde{\sigma}_{\mathrm{ICI}}^2$ increasing. For 4-QAM, the case of N = 128 shows higher error, compared with the case of N = 32, due to larger $\tilde{\sigma}_{\mathrm{ICI}}^2$. However, the error reduces from N = 32 to N = 128 for 64-QAM owing to the reduction of $\gamma_{2,\mathrm{ICI}}$. Furthermore, although the dispersion-induced ICI is assumed to be Gaussian-distributed to estimate theoretical BER in direct-detection optical OFDM systems [10], the underestimation of BER increases after longer transmission distance corresponding to the higher power and the higher kurtosis of ICI.

4. Using *t*-distribution to simulate ICI

From Figs. 5-7, it is evident that assuming ICI to be Gaussian distributed is not precise. While the kurtosis excess can be computed by Eq. (12), a known distribution with adjustable kurtosis and zero skewness may be utilized to approach the exact distribution. A good candidate in the Pearson system is the Pearson type VII distribution [18], i.e. the well-known *t*-distribution, of which the normalized probability density function (pdf) is,

$$p_\nu(x) = \frac{\Gamma\left(\frac{\nu+1}{2}\right)}{\sqrt{\pi(\nu-2)}\,\Gamma\left(\frac{\nu}{2}\right)}\left(1+\frac{x^2}{\nu-2}\right)^{-\frac{\nu+1}{2}}, \tag{17}$$

and $\Gamma(x)$ is the Gamma function. The variance and kurtosis excess of $p_\nu(x)$ are 1 and $6/(\nu-4)$, respectively. While ν approaches infinity, kurtosis excess is zero and it becomes a normal distribution. By setting $\nu = 4 + 6/\gamma_{2,\mathrm{ICI}}$, the corresponding CDFs of the *t*-distribution are plotted by the dashed lines in Fig. 6(b), and the *t*-distributions have good agreement with the numerical results. To further examine the similarity between the *t*-distribution and ICI distribution, Eq. (10) is used to calculate BER curves, and the theoretical BER becomes Eq. (6) after replacing $\mathrm{Q}(x)$ by $\mathrm{T}(x, \nu_W)$ [18]:

$$\mathrm{T}(x,\nu_W) = \frac{1}{2} - \frac{x\,\Gamma\left(\frac{\nu_W+1}{2}\right)}{\sqrt{\pi(\nu_W-2)}\,\Gamma\left(\frac{\nu}{2}\right)}\,{}_2F_1\left(\frac{1}{2},\frac{\nu_W+1}{2};\frac{3}{2};\frac{-x^2}{\nu_W-2}\right), \tag{18}$$

where ${}_2F_1(a_1,a_2;b;z)$ is the hypergeometric function, and ν_W is a modified parameter to describe the variation of kurtosis excess thanks to the combination of ICI and white noise. Assuming A and B are two independent real random variable with the means of zero, the

#133218 - $15.00 USD Received 11 Aug 2010; revised 7 Sep 2010; accepted 7 Sep 2010; published 15 Sep 2010

variances of σ_a^2 and σ_b^2 and the kurtosis excesses of $\gamma_{2,a}$ and 0, respectively, the kurtosis excess of their summation is,

$$\frac{\left\langle (a+b)^4 \right\rangle}{\left\langle (a+b)^2 \right\rangle^2} - 3 = \frac{\left\langle a^4 \right\rangle + \left\langle b^4 \right\rangle + 6\left\langle a^2 \right\rangle \left\langle b^2 \right\rangle}{\left\langle a^2 \right\rangle^2 + \left\langle b^2 \right\rangle^2 + 2\left\langle a^2 \right\rangle \left\langle b^2 \right\rangle} - 3 = \frac{\gamma_{2,a}\sigma_a^4}{\left(\sigma_a^2 + \sigma_b^2\right)^2}.$$

If *A* and *B* represents ICI and white noise, respectively, the modified parameter, ν_W, can be written as,

$$\nu_W = 4 + \frac{6}{\gamma_{2,\mathrm{ICI}}(q)}\left(1 + \frac{1}{\rho\,\tilde{\sigma}_{\mathrm{ICI}}^2(q)}\right)^2. \tag{19}$$

For comparison, the BER curves calculated from Eqs. (13) and (18) are shown in Fig. 3, and the *t*-distibution can fit the simulation results well. Figures 8-11 exhibit the SNR penalty at the BER of 10^{-3}. Only ICI is considered in Figs. 8-11(b), and only PRT is considered in Figs. 8-11(c), while both of them are included in Figs. 8-11(a). Figures 8-11(c) depict that the penalty induced by PRT can be estimated well by Eq. (6) by setting $\tilde{\sigma}_{\mathrm{ICI}}^2 = 0$, although it slightly overestimates. However, compared with the numerical results, Gaussian approximation of ICI will underestimate BER, and therefore, overestimate the maximum transmission distance as shown in Fig. 8-11(a). While the distribution of ICI is approximated by *t*-distribution, it shows estimation error of < 1 dB with or without considering PRT. However, if the laser linewidth is wider and/or the higher order QAM is adopted, the maximum transmission distance and the accumulated CD are lower, and the corresponding power and kurtosis of ICI are also lower resulting in smaller estimation error by Gaussian approximation, such as the case shown in Figs. 11(a) and (b). In conclusion, *t*-distribution offers a simple and reasonable way to estimate the BER and the maximum transmission distance limited by dispersion-induced PN, especially when the subcarrier number is low and the accumulated CD is high.

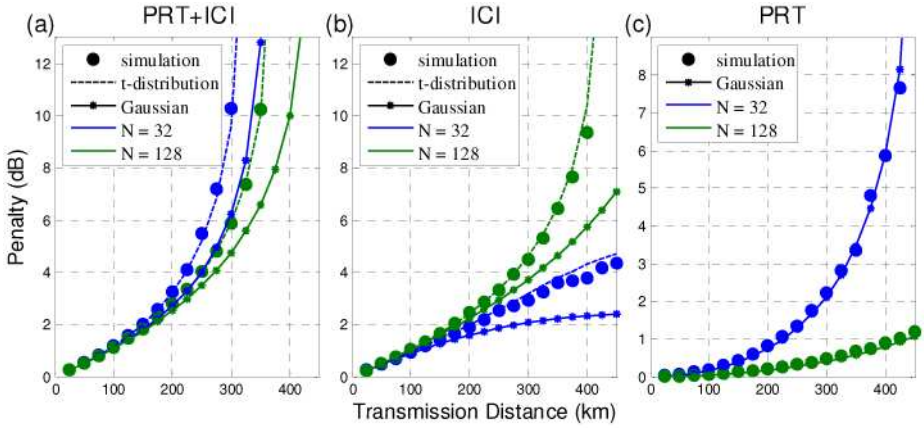

Fig. 8. SNR penalty as a function of transmission distance for 16-QAM OFDM signals with 1-MHz laser linewidth

#133218 - $15.00 USD Received 11 Aug 2010; revised 7 Sep 2010; accepted 7 Sep 2010; published 15 Sep 2010

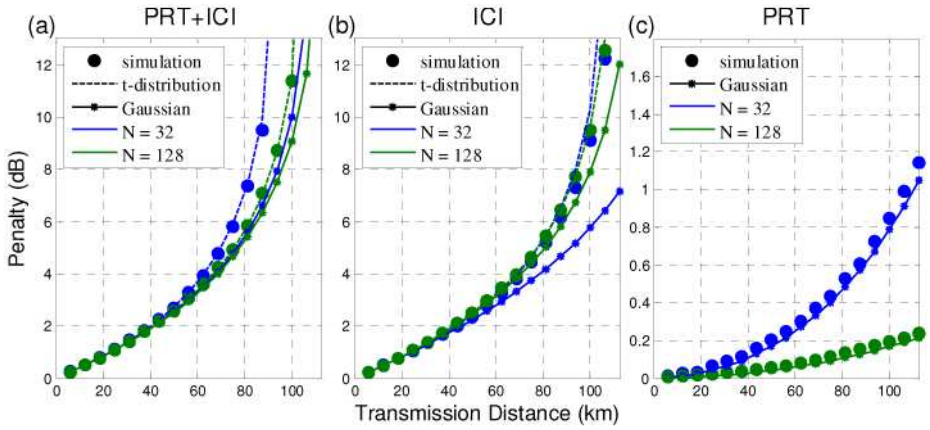

Fig. 9. SNR penalty as a function of transmission distance for 64-QAM OFDM signals with 1-MHz laser linewidth

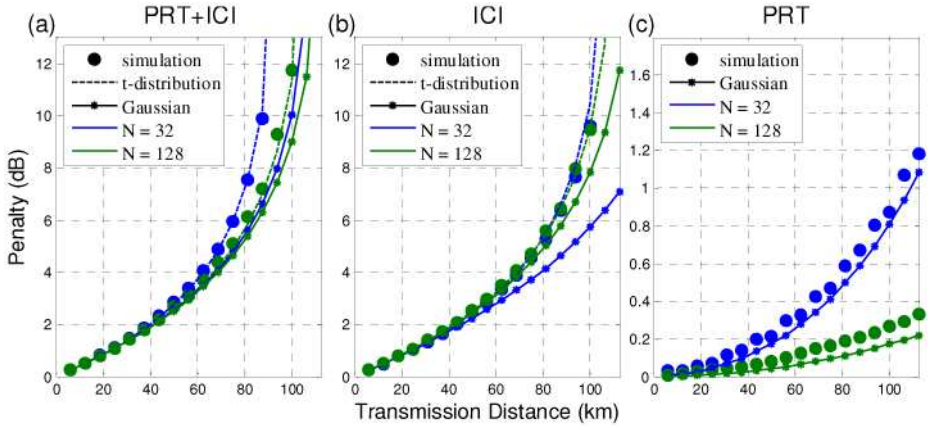

Fig. 10. SNR penalty as a function of transmission distance for 16-QAM OFDM signals with 4-MHz laser linewidth

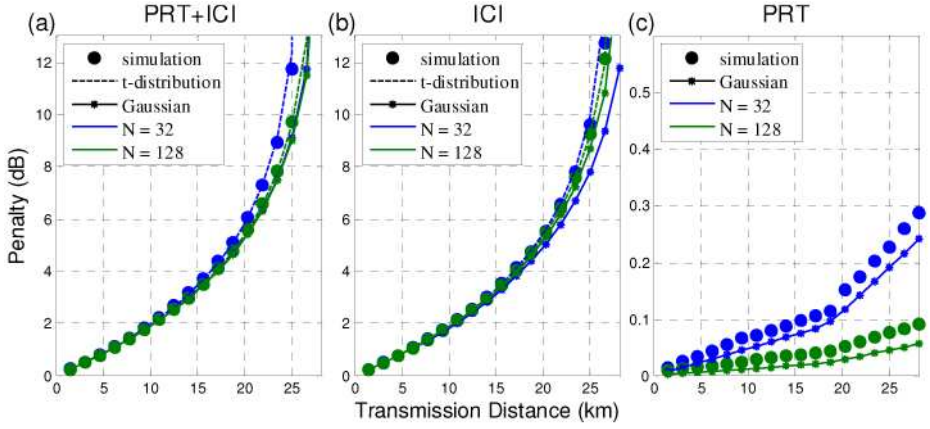

Fig. 11. SNR penalty as a function of transmission distance for 64-QAM OFDM signals with 4-MHz laser linewidth

#133218 - $15.00 USD Received 11 Aug 2010; revised 7 Sep 2010; accepted 7 Sep 2010; published 15 Sep 2010

5. Conclusions

This work studies the effect of PN induced by CD on OFDM RoF systems at 60-GHz band. The powers of PRT and ICI are calculated analytically, and ICI is shown to be non-Gaussian distributed by computing its Kurtosis excess. We also show the estimation error of Gaussian approximation increases, when the subcarrier number decreases and the transmission distance increases. To estimate the penalty induced by ICI, *t*-distribution is adopted to approach the exact distribution of ICI owing to its adjustable kurtosis. Compared with the numerical results, the approximation of *t*-distribution can provide a simple way to calculate the BER with estimation error of < 1 dB under different laser linewidths, subcarrier numbers, modulation formats, and transmission distances.

#133218 - $15.00 USD Received 11 Aug 2010; revised 7 Sep 2010; accepted 7 Sep 2010; published 15 Sep 2010